Available online at www.sciencedirect.com

ScienceDirect

Polar Science 8 (2014) 129–145

http://ees.elsevier.com/polar/

Column-averaged CO_2 concentrations in the subarctic from GOSAT retrievals and NIES transport model simulations

D.A. Belikov [a,b,e,*], A. Bril [b], S. Maksyutov [b], S. Oshchepkov [b], T. Saeki [b,1], H. Takagi [b], Y. Yoshida [b], A. Ganshin [c], R. Zhuravlev [c], S. Aoki [d], T. Yokota [b]

[a] *Division for Polar Research, National Institute of Polar Research, Tokyo, Japan*
[b] *Center for Global Environmental Research, National Institute for Environmental Studies, Tsukuba, Japan*
[c] *Central Aerological Observatory, Dolgoprudny, Russia*
[d] *Center for Atmospheric and Oceanic Studies, Graduate School of Science, Tohoku University, Sendai, Japan*
[e] *Tomsk State University, Tomsk, Russia*

Received 21 March 2013; revised 17 February 2014; accepted 21 February 2014
Available online 12 March 2014

Abstract

The distribution of atmospheric carbon dioxide (CO_2) in the subarctic was investigated using the National Institute for Environmental Studies (NIES) three-dimensional transport model (TM) and retrievals from the Greenhouse gases Observing SATellite (GOSAT). Column-averaged dry air mole fractions of subarctic atmospheric CO_2 (XCO_2) from the NIES TM for four flux combinations were analyzed. Two flux datasets were optimized using only surface observations and two others were optimized using both surface and GOSAT Level 2 data. Two inverse modeling approaches using GOSAT data were compared. In the basic approach adopted in the GOSAT Level 4 product, the GOSAT observations are aggregated into monthly means over $5^\circ \times 5^\circ$ grids. In the alternative method, the model–observation misfit is estimated for each observation separately. The XCO_2 values simulated with optimized fluxes were validated against Total Carbon Column Observing Network (TCCON) ground-based high-resolution Fourier Transform Spectrometer (FTS) measurements. Optimized fluxes were applied to study XCO_2 seasonal variability over the period 2009–2010 in the Arctic and subarctic regions. The impact on CO_2 levels of emissions from enhancement of biospheric respiration induced by the high temperature and strong wildfires occurring in the summer of 2010 was analyzed. Use of GOSAT data has a substantial impact on estimates of the level of CO_2 interanual variability.

Keywords: Carbon cycle; Atmospheric transport; Inverse modeling; GOSAT

1. Introduction

Arctic and subarctic regions are large carbon reservoirs. Permafrost soils covering about 25% of the land surface in the Northern Hemisphere store nearly twice as much carbon as is currently present in the atmosphere (Brown et al., 1997; Schuur et al., 2009).

* Corresponding author. Center for Global Environmental Research, National Institute for Environmental Studies, Tsukuba, Japan.
E-mail address: dmitry.belikov@nies.go.jp (D.A. Belikov).
[1] Present address: Japan Agency for Marine-Earth Science and Technology, Yokohama, Japan.

http://dx.doi.org/10.1016/j.polar.2014.02.002
1873-9652/

Schuur et al. (2009) found that areas which have thawed over the last 15 years show annual losses of old carbon that are 40% greater than those observed in minimally thawed areas, while areas that thawed decades earlier show annual old carbon losses 78% greater than those observed in minimally thawed areas. Organic carbon in permafrost soils may act as a positive feedback to global climate change due to enhanced biospheric respiration rates with warming (Koven et al., 2011).

A comparison of observations performed in 1958–1961 and 2009–2011 reveals a strikingly large (~50%) increase of atmospheric CO_2 seasonal amplitude north of 45°N, which must be attributed almost entirely to the terrestrial biosphere activity (Graven et al., 2013). None of the terrestrial ecosystem models currently participating in the fifth phase of the Coupled Model Intercomparison Project (CMIP5) can account for the increase in CO_2 amplitude. However, there is a high degree of uncertainty regarding the rate of carbon release due to permafrost thaw, microbial decomposition of previously frozen organic carbon, and terrestrial biosphere activity. Moreover, the scarcity of observations in subarctic regions means that the carbon cycle there is not well monitored.

Inverse modeling of carbon exchange at the Earth's surface allows quantification of the spatial distribution of terrestrial carbon sources and sinks, and their seasonal to interannual variability, as shown by Bousquet et al. (2000) and Peters et al. (2007), among others. However, at global scales, many gaps in atmospheric CO_2 measurements remain in remote areas that are geographically distant from CO_2 observation networks, especially at high latitudes in the Northern Hemisphere, thus giving rise to large uncertainties in the estimated fluxes (Gloor et al., 2000). These gaps can be filled using satellite observations of atmospheric CO_2 concentrations (Rayner and O'Brien, 2001). The Thermal And Near-infrared Sensor for carbon Observation–Fourier Transform Spectrometer (TANSO–FTS) onboard the Greenhouse gases Observing SATellite (GOSAT) has been designed to fill gaps in ground-based observation networks through space-based monitoring of the global distribution of greenhouse gases (CO_2 and CH_4) (Kuze et al., 2009; Yokota et al., 2009). The GOSAT column-averaged dry air mole fractions of atmospheric CO_2 (XCO_2) data are expected to contribute to accurate estimates of the global carbon budget because of wide spatial coverage and high temporal resolution of the data. Although retrieval algorithms are still under development (Oshchepkov et al., 2012), the first CO_2 inverse modeling studies using GOSAT data have been completed (Takagi et al., 2011; Basu et al., 2013; Maksyutov et al., 2013; Saeki et al., 2013). The combined use of GOSAT data and surface measurements leads to a reduction in CO_2 flux uncertainties in some tropical and remote land regions, as compared with data based on surface measurements alone (Takagi et al., 2011; Maksyutov et al., 2012; Saeki et al., 2013).

Guerlet et al. (2013) used XCO_2 measured by GOSAT to reveal significant interannual variations (IAV) in CO_2 uptake during the Northern Hemisphere summer during 2009 and 2010. The reduced carbon uptake in the summer of 2010 is most likely due to the heat wave in Eurasia and fire emissions in the Northern Hemisphere, especially in central western Russia. Although wildfires occurred mainly in the forest zone (52°–58°N, 33°–43°E; Witte et al., 2011), the persistent southerly flow transported air into central and northern Europe (Grumm, 2011). During this period, huge amounts of aerosols, CO, CO_2, and other substances were released into the atmosphere as a result of biomass burning (Konovalov et al., 2011; Sitnov, 2011; Muskett, 2013). The smoke drifted long distances with air masses, and on several occasions it could be observed in Eastern Finland (Portin et al., 2012).

The transport of enhanced CO_2 should be accompanied by large amounts of other combustion products, including CO and aerosols. Smoke particles have a significant impact on the earth's radiation balance, especially in the Arctic. When present in the atmosphere, smoke particles may contribute as much as 20% to the aerosol optical thickness during summertime due to dispersion and absorption of solar radiation (Reid et al., 2005; Barnaba et al., 2011). On the ground, when deposited on snow, they have a considerable effect on surface albedo (Stohl et al., 2006, 2007). Thus, the impact of forest fires in central western Russia to the Arctic and subarctic regions are many-faceted and require further study.

In this work, we use forward simulation employing the National Institute for Environmental Studies (NIES) three-dimensional transport model (TM) and GOSAT retrieval data to analyze the distribution of XCO_2 in the subarctic. We study XCO_2 seasonal variability for the period 2009–2010 and discuss the impact of emissions from strong wildfires occurring in the summer of 2010 in central western Russia, the USA, and Canada on enhanced CO_2 concentrations in the Arctic and subarctic

regions. The remainder of the paper is organized as follows. Section 2 briefly describes GOSAT observations and the model components; Section 3 introduces the results and gives a discussion; and Section 4 presents conclusions.

2. Method

2.1. GOSAT XCO_2 retrievals

The GOSAT satellite was launched on 23 January 2009 to monitor the global distributions of greenhouse gases (CO_2 and CH_4) from space. The satellite is in a sun-synchronous orbit with an equator crossing time of about 13:00 local time and an inclination angle of 98°. The satellite flies at an altitude of approximately 666 km, completes an orbit in about 100 min, and operates on a global basis with a 3-day repeat cycle.

The nadir-looking TANSO-FTS is the main instrument aboard GOSAT. It measures surface-reflected sunlight and emitted thermal infrared radiation at wavelengths in the range 0.76–14.3 μm. The TANSO-FTS obtains data in three narrow bands in the short wavelength infrared region (band centers at 0.76, 1.6, and 2.0 μm; also referred to as TANSO-FTS bands 1, 2, and 3, respectively) and is sensitive to the total column CO_2 between the surface and the top of the atmosphere within its footprint area of ~80 km^2. The sensitivity change with height can be taken into account using column averaging kernels. The design and functions of the instrument are described in detail by Kuze et al. (2009).

Several retrieval algorithms have been developed by different research groups for routinely processing GOSAT observational data (Oshchepkov et al., 2013). In this study, we use the GOSAT Level 2 (L2) XCO_2 retrieval (version 02.00) dataset (Yoshida et al., 2011, 2012, 2013) distributed to general users for comparisons with model results; this GOSAT dataset was also used in the inversion model to yield optimized fluxes (Maksyutov et al., 2013).

2.2. NIES transport model

The NIES TM is designed to simulate natural and anthropogenic synoptic-scale variations in atmospheric constituents on diurnal, seasonal, and interannual timescales. The model uses a mass-conservative flux-form formulation that consists of a third-order van Leer advection scheme (van Leer, 1977) and a horizontal dry-air mass flux correction. The horizontal latitude–longitude grid is a reduced rectangular grid (Heimann and Keeling, 1989), with a spatial resolution of 2.5° × 2.5° near the equator (Belikov et al., 2011). The model is off-line and is driven by a dataset that consists of both Japanese 25-yr Reanalysis (JRA-25) and Japan Meteorological Agency Climate Data Assimilation System (JCDAS) data (Onogi et al., 2007). The JRA-25/JCDAS data are available on Gaussian horizontal grid T106 with 40 hybrid $\sigma-p$ levels every 6 h. Thus, the model integration time step is also 6 h.

The present version of the model (NIES-08.1i) uses a flexible hybrid sigma–isentropic ($\sigma-\theta$) vertical coordinate that consists of terrain-following and isentropic levels switched smoothly near the tropopause. Vertical transport in the stratosphere is controlled by the climatological heating rate derived from the JRA-25/JCDAS reanalysis dataset (Belikov et al., 2013b).

Parameterization of turbulent diffusivity follows the approach used by Hack et al. (1993), with transport processes in the planetary boundary layer (PBL) and free troposphere evaluated separately. Three-hourly PBL heights are taken from the European Centre for Medium-Range Weather Forecasts (ECMWF) ERA-Interim reanalysis dataset. We use a modified Kuo-type cumulus convection parameterization scheme (Belikov et al., 2013a), which computes the mass of air transported upward in a cumulus cell using conservation of moisture and a detailed distribution of convective precipitation provided by the JRA-25/JCDAS reanalysis data.

2.3. NIES TM simulation setup

To simulate XCO_2, the NIES TM was run for the period from 1 January 2009 to 31 December 2010, employing the initial global XCO_2 distribution derived from GLOBALVIEW-CO2 (2011). Four cases with different source components of CO_2 were considered in this study. Two flux sets were optimized without GOSAT data and two others were optimized with GOSAT retrieval data:

2.3.1. Prior + GV

This flux set was obtained using the region-based inverse modeling scheme designed in the Transcom project (i.e., Gurney et al., 2002). The *a priori* fluxes were optimized with a 3-month window fixed-lag Kalman smoother inverse modeling system (Takagi et al., 2011; Maksyutov et al., 2012). Monthly fluxes for 42 sub-continental terrestrial regions and 22 oceanic basins, as defined by Patra et al. (2005), were inferred for the 12 months from June 2009 to May 2010, using

GLOBALVIEW (hereafter denoted as GV) observations collected from existing surface and aircraft CO_2-measurement networks (GLOBALVIEW-CO2, 2011). The CO_2 fields used in the inversions were calculated using the NIES TM. The *a priori* flux dataset used as a first guess for the inverse modeling to drive the atmospheric transport model consists of four components (Takagi et al., 2011; Maksyutov et al., 2012): (a) fossil fuel and cement manufacturing emissions from the high-resolution Open source Data Inventory of Anthropogenic CO_2 (ODIAC) dataset (Oda and Maksyutov, 2011), and the Carbon Dioxide Information Analysis Center's (CDIAC) dataset (Andres et al., 2009, 2011); (b) daily net ecosystem exchange (NEE) simulated by the Vegetation Integrative SImulator for Trace gases (VISIT) terrestrial biosphere model (Ito, 2010; Saito et al., 2011, 2013); (c) monthly air–sea CO_2 fluxes predicted by an ocean pCO_2 data assimilation system based on the Offline ocean Tracer Transport Model (OTTM; Valsala and Maksyutov, 2010); and (d) monthly CO_2 emissions due to biomass burning from the Global Fire Emissions Database (GFED) version 3.1 (van der Werf et al., 2010).

2.3.2. *Prior + GV + GOSAT*

These fluxes were optimized using the same inverse modeling system as that used in the Prior + GV case, but both GLOBALVIEW observations and the GOSAT Level 2 XCO_2 retrieval data (version 02.00) covering 14 months from June 2009 to July 2010 are used. In this setup, GOSAT XCO2 retrievals were aggregated over each 5° × 5° grid cell and over each month. Details are given by Takagi et al. (2011) and Maksyutov et al. (2013). Presently Prior + GV + GOSAT data as well as Prior + GV fluxes are available for period June 2009 − October 2010. To cover gaps in NIES TM simulation period (1 January 2009 to 31 December 2010) we used unoptimized *a priori* fluxes.

2.3.3. *LMDZ*

The 3-hourly inverse-model-adjusted fluxes obtained by optimizing the surface fluxes of CO_2 using the LMDZ model for the period 2000–2010 on a 3.75° × 2.5° latitude–longitude grid (Chevallier et al., 2010). The fluxes comprise assimilated observations from 128 stations from three large datasets of measurements of the surface CO_2 mixing ratio. These data sources, representing cooperative efforts from many laboratories around the globe, are: the NOAA ESRL archive (ftp://ftp.cmdl.noaa.gov/ccg/co2/), the CarboEurope atmospheric archive (http://ceatmosphere.lsce.ipsl.fr/database/index_database.html), and the WDCGG archive (http://gaw.kishou.go.jp/cgi-bin/wdcgg/catalogue.cgi) (Chevallier et al., 2010).

2.3.4. *GELCA-EOF*

These fluxes are obtained using a combination of Global Eulerian–Lagrangian Coupled Atmospheric (GELCA) model and an EOF-based method (Zhuravlev et al., 2013). An empirical orthogonal function (EOF)-based inverse modeling scheme relying on the derivation of a limited set of spatial functions that can represent major components of surface flux variability (Zhuravlev et al., 2011). Here, we used 137 EOF components for land and 87 components for ocean, and we found that several tens of derived base functions are sufficient to achieve almost full reduction of the model–observation misfit, with the number of control variables comparable to a region-based approach. The advantage of this approach over a region-based approach is that the base functions are smooth and follow ecosystem type distributions and climate variation patterns (Maksyutov et al., 2013). The tracer transport is simulated with GELCA model (Ganshin et al., 2012), which combines the Lagrangian Flexpart model at a resolution of 1.25° × 1.25° (Stohl et al., 2005) with the Eulerian NIES TM model. A priori fluxes were the same as in the Prior + GV setup. To solve the inverse problem, a fixed-lag Kalman smoother was used with a 4-month window. Ground-based observations for 60 sites were taken from the open access NOAA database for 2009–2010. Column values of CO_2 used in this setup were also retrieved using the GOSAT L2 method, as in the Prior + GV + GOSAT case, but in contrast to Prior + GV + GOSAT, single-shot observations were assimilated separately using the corresponding averaging kernels prepared by data providers.

2.4. *Analysis of XCO_2 derived from NIES TM and GOSAT retrievals over the globe*

This paper is concentrated on study of XCO_2 in arctic and subarctic regions. The global XCO_2 values predicted by the NIES TM and retrieved using GOSAT L2 algorithms were analyzed in previous studies (Belikov et al., 2013b; Oshchepkov et al., 2012, 2013). Validation was performed against the reference data collected by ground-based high-resolution Fourier Transform Spectrometers (FTS) installed at the monitoring sites of the Total Carbon Column Observing Network (TCCON) (Wunch et al., 2011).

For comparison with TCCON FTS observations, the NIES TM model was run with only *a priori* (Section

2.3) unoptimized CO_2 fluxes that combine fossil fuel, land, and ocean sources and sinks (Belikov et al., 2013b). We selected simulated and TCCON XCO_2 taken at around 13:00 ± 1 h local time over twelve TCCON sites for the period January 2009 to January 2011. We considered data from three sites in the Southern Hemisphere (Darwin, Lauder, and Wollongong) and nine from the Northern Hemisphere (Bialystok, Bremen, Garmisch, Izãna, Lamont, Orleans, Park Falls, Sodankylä, and Tsukuba). The NIES TM is able to reproduce seasonal and interannual variability of XCO_2 with correlation coefficients of 0.8–0.9 and general biases of about ±1.2 ppm for XCO_2 against version GGG-2012 TCCON data (Belikov et al., 2013b).

Oshchepkov et al. (2012, 2013) performed a comparative analysis of XCO_2 retrievals from six global algorithms, including GOSAT NIES Level 2 v. 02.00, against TCCON FTS observations for the period from June 2009 to December 2010. The pattern of small seasonal variations in the retrieved XCO_2 is generally in line with that of the ground-based FTS. The NIES Level 2 v. 02.00 and TCCON XCO_2 data yielded a correlation coefficient of 0.88, standard deviation of 1.68 ppm, and a negative bias (Level 2 v. 02.00 − TCCON) of −1.07 ppm for measurements over 11 stations (Oshchepkov et al., 2013). Thus, the two comparisons show better agreement of NIES TM model-based XCO_2 with TCCON in reproducing the seasonal cycle and less scatter than between the GOSAT NIES Level 2 v. 02.00 retrieval algorithm and TCCON.

3. Results

3.1. Distribution of XCO_2 in subarctic regions

We selected the summer months to analyze the distribution of XCO_2 in subarctic regions because this season is characterized by significant temporal variability, specifically with respect to XCO_2 reduction at high latitudes on account of CO_2 uptake by the biosphere. Figs. 1 and 2 show comparisons of XCO_2 derived by NIES TM (Prior + GV) and GOSAT L2 in the Northern Hemisphere for June and August 2009, respectively. The GOSAT satellite can measure in two modes: observation over land at lattice points, and in sun-glint mode over the sea. However, sun-glint observations are only possible in tropical regions (latitudes below 30°), where the solar zenith angle is sufficiently small. In subarctic regions only observations over land are available. Figs. 1 and 2 show XCO_2 values only for coincident points of GOSAT and the model. Note that modeled XCO_2 was selected for all GOSAT scans, but during retrieval processing of GOSAT XCO_2, some satellite data points were filtered out (over Greenland and coastal regions). Therefore, 6071 and 6817 GOSAT scans are available for June and August, respectively. The GOSAT observations show much higher spatial variations than modeled XCO_2, because they are usually contaminated by aerosol and cloud (Oshchepkov et al., 2012, 2013). Nevertheless, the differences between GOSAT L2 and NIES TM results are mostly within 2.5 ppm (∼0.5%) globally (Oshchepkov et al., 2013).

3.2. Comparison of XCO_2 derived from NIES TM and TCCON FTS

Here, we repeated the comparison of modeled XCO_2 with TCCON data. The CO_2 fluxes were evaluated by incorporating them into the NIES TM and sampling the model at the location and time of XCO_2 measurements from ground-based high-resolution FTS observations collected at two of the northernmost TCCON sites, Ny Ålesund (Norway, 78.92°N, 11.92°E) and Sodankylä (Finland, 67.37°N, 26.63°E); site locations are shown on Figs. 1 and 2. Another northern site, Eureka (Canada, 80.05°N, 86.42°W), was recently established, but available data are insufficient for the period under consideration. To show the effects of adding GOSAT retrievals to the ground-based observations on the seasonality of the estimated fluxes, we plotted time-series of XCO_2 from the model and the FTS sites (Fig. 3). The XCO_2 model offsets (∼1 ppm) were adjusted following Belikov et al. (2013a) to match the global total fossil fuel emission.

The correlation coefficients (0.98–0.99) and biases (0.40–1.33 ppm) presented in Table 1 show that the use of optimized fluxes improved XCO_2 simulations for the two TCCON FTS sites as compared with previous analyses using unoptimized data (Belikov et al., 2013b). Adding GOSAT retrievals to the inversion does not give a major improvement for this region, as shown by comparing Prior + GV with Prior + GV + GOSAT. This is mainly because local fluxes from regions near TCCON sites are well constrained by ground-based CO_2 observations, which are more accurate than GOSAT data. However, this only applies to a limited number of regions, mainly those located in areas with good surface observational coverage. The high resolution GELCA-EOF inversion system based on the coupled Eulerian–Lagrangian model gives lower

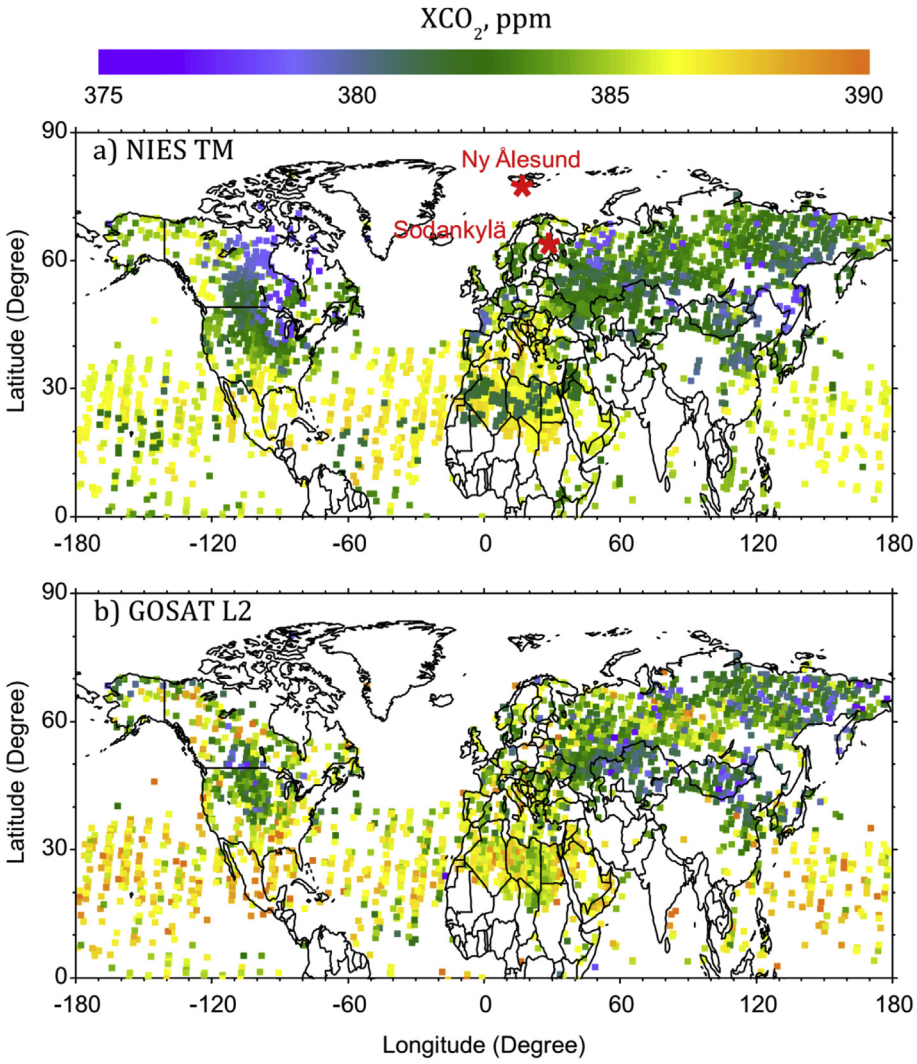

Fig. 1. Northern Hemisphere maps of monthly mean XCO_2 (ppm) from NIES TM (top) and GOSAT L2 data (bottom) for June 2009. The data are averaged over 2.5° × 2.5° latitude–longitude grid boxes. Red symbols show the locations of the TCCON FTS stations at Ny Ålesund (Norway, 78.92°N, 11.92°E) and Sodankylä (Finland, 67.37°N, 26.63°E).

biases (0.40–0.53), demonstrating its advantages over a region-based approach.

Profile of XCO_2 calculated with Prior + GV and LMDZ fluxes are in good agreement to each other (Table 1), apparently because correspondent fluxes was optimized with similar sets of surface observations.

3.3. Seasonal cycle of XCO_2 derived for latitude bands in subarctic regions

Given the small number of GOSAT observations, we averaged the data over 5° latitudinal bands from 55°N to 75°N to evaluate the Northern Hemisphere seasonal cycle of carbon dioxide. The GOSAT XCO_2 values were compared with those from NIES TM (Prior + GV, Prior + GV + GOSAT, LMDZ, and GELCA-EOF flux combinations). We only selected those NIES TM data points that were coincident with GOSAT observations. We also averaged all data over 3 days, which is the GOSAT repeat cycle, as this reduces errors for scans obtained from nearby areas.

The XCO_2 fields simulated with Prior + GV and LMDZ fluxes are compared directly with GOSAT data, because only these combinations were optimized without GOSAT. High-latitude GOSAT data over land are only available for the summer season, as the solar zenith angle is too large at other times. Therefore, the duration of available data decreases with latitude. It is

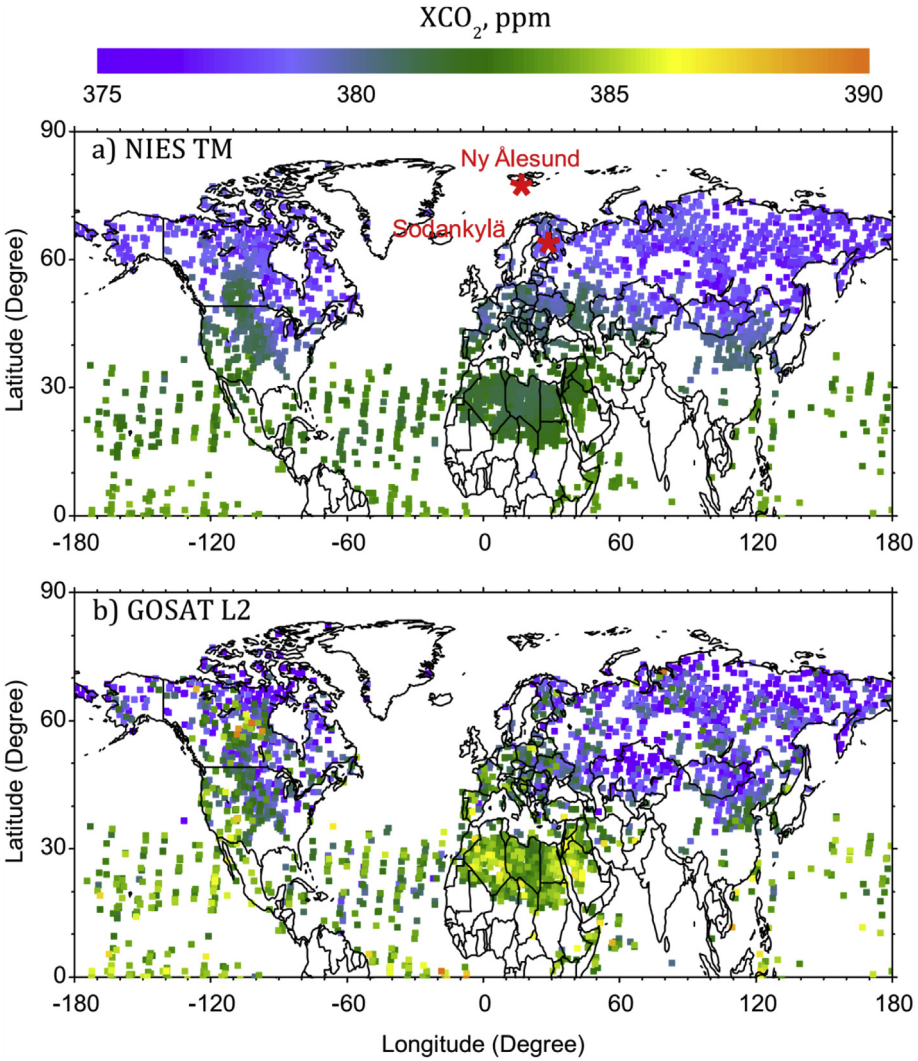

Fig. 2. Same as Fig. 1, but for August 2009.

obvious that the temporal data coverage is best in the 55°–60°N band (Fig. 4). However, the number of measurements is greatest in the 60°–65°N band (Table 2), as this band has more days with clear sky conditions than do other selected bands. In general, the NIES TM is able to describe the seasonal cycle quite clearly, as fluxes were optimized for 2009–2010. The difference between the modeled profiles is minor. NIES TM with LMDZ fluxes are slightly better in describing GOSAT XCO2 features (i.e. August (Fig. 4b) and September (Fig. 4a) of 2010), as these fluxes benefit from a 3-hourly temporal resolution. Better temporal resolution helps to resolve the diurnal cycle of CO_2, which is influenced by boundary layer variability, wind speed, and other weather conditions.

The correlation coefficient is quite high for all bands (>0.9), apart from the northernmost band, for which it dropped to 0.87–0.95. The number of GOSAT scans decreases, and the errors associated with a low zenith angle increase, towards the North Pole; consequently, the bias reaches maximum values of 2.99 and 3.28 ppm respectively at the latitudinal band 70–75°N. This mainly explains why the average bias values of 1.70 and 1.94 ppm exceed the current precision of GOSAT data (~±1 ppm; Cogan et al., 2012); however, the agreement with modeled results is quite reasonable over this large area, which is not covered by any other measurements.

Assessment of the XCO_2 seasonal cycle amplitude for the selected period (2009–2010) is difficult, as

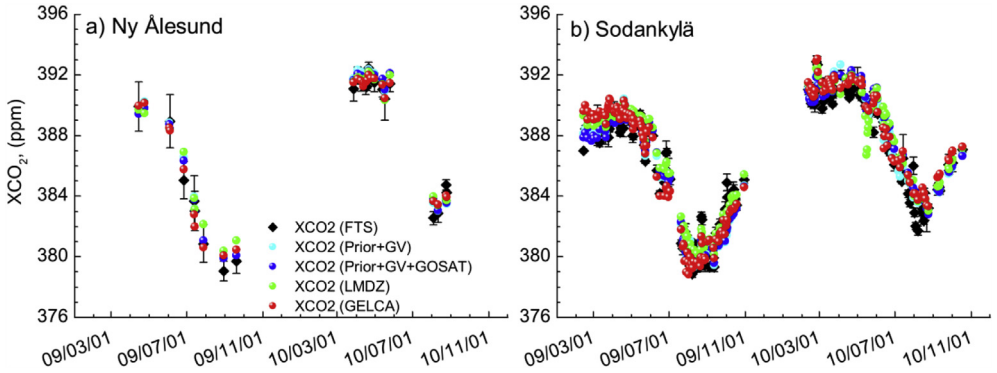

Fig. 3. Time series of XCO_2 measured by FTS and modeled by NIES TM using Prior + GV (cyan), Prior + GV + GOSAT (blue), LMDZ (green) and GELCA-EOF (red) fluxes for a) Ny Ålesund (Norway, 78.92°N, 11.92°E) and b) Sodankylä (Finland, 67.37°N, 26.63°E) TCCON sites. The error bar for the FTS points is a combination of the spread due to weighted averaging within the 13:00 ± 1 h local time interval and observation error. (For interpretation of the references to color in this figure legend, the reader is referred to the web version of this article.)

only part of the seasonal data is available. Moreover, a marked difference in the northern extra-tropical summer CO_2 uptake between 2009 and 2010 was revealed. It was found the XCO_2 drawdown in 2010 was lower than that in 2009, by 2.4 ppm and 3.0 ppm over North America and Eurasia, respectively (Guerlet et al., 2013). Nevertheless, we can estimate the difference in the amplitude of the XCO_2 seasonal cycle from modeled and retrieved distributions.

In general, the model using Prior + GV, Prior + GV + GOSAT, LMDZ, and GELCA-EOF fluxes seriously underestimated the XCO_2 seasonal cycle amplitude (Table 3). The modeled amplitudes are lower than observed amplitudes by 1–4 ppm, due mainly to the model's inability to reproduce a summer reduction in concentration caused by biospheric carbon uptake. It is unclear which factors play a major role in this regard, whether transport model errors or flux drawbacks.

The simulation using the GELCA-EOF flux is in best agreement with observations among the modeled XCO_2 for 2009, and is in worse agreement for 2010. Use of Prior + GV + GOSAT fluxes leads to degradation of amplitude values in comparison with the design without GOSAT L2 (Prior + GV). Thus, implementation of GOSAT data in the inversion has an unstable impact on the amplitude of XCO_2 and is very sensitive to the inversion technique, the transport model used for forward simulation, and also to bias correction and data filtering (Maksyutov et al., 2012).

Prior + GV and LMDZ fluxes were obtained using completely different variational methods and sets of observation network sites. Moreover LMDZ dataset was inverted using different transport model, as result is was not specially optimized for NIES TM. Thus, consistency of XCO_2 profiles calculated using these fluxes (Table 1) is important indicator of the results reliability.

Table 1
Correlation coefficients and biases for the modeled XCO_2 for the Ny Ålesund and Sodankylä TCCON sites, using Prior + GV, Prior + GV + GOSAT, LMDZ, and GELCA-EOF fluxes for 2009–2010.

Flux combination	Correlation coefficient		Average bias, ppm	
	Ny Ålesund	Sodankylä	Ny Ålesund	Sodankylä
Prior + GV	0.99	0.98	1.04	0.80
Prior + GV + GOSAT	0.99	0.98	1.33	1.18
LMDZ	0.99	0.98	0.95	1.08
GELCA-EOF	0.99	0.98	0.40	0.53

3.4. Analysis of reduced carbon uptake during the summer of 2010

The summer of 2010 was characterized by reduced carbon uptake, which is most likely due to the heat wave in Eurasia driving biospheric fluxes and fire emissions (Guerlet et al., 2013). Strong forest fires occurred in the Northern Hemisphere, including in Canada and Russia, as shown by the GFED forest fire product (Fig. 5). The 2010 Russian wildfires spread dangerously towards populated regions, significantly affecting human health and livelihood. The prolonged anti-cyclonic circulation established over western parts of Russia (near Moscow in July–August) favored the development of mass forest and peat bog fires (Grumm, 2011). The persistent southerly flow transported large amounts of combustion products,

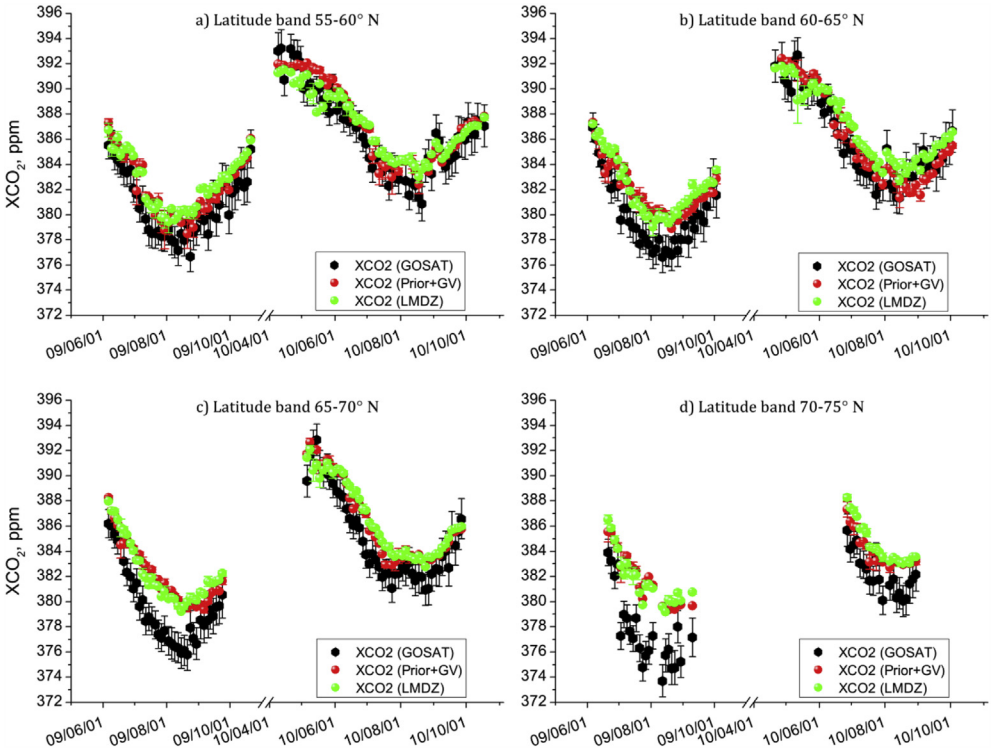

Fig. 4. Time series of XCO_2 from GOSAT L2 (black) and NIES TM with Prior + GV (green) and LMDZ (red) fluxes for 2009 for different latitude bands over land in the Northern Hemisphere: a) 55°–60°N, b) 60°–65°N, c) 65°–70°N, and d) 70°–75°N. (For interpretation of the references to color in this figure legend, the reader is referred to the web version of this article.)

including CO_2, into central and northern Europe, generating an extended area of enhanced CO_2 concentrations. The difference in XCO_2 between 2010 and 2009 for the period June–October, averaged over 5° bands, is shown in Fig. 6 (the data have been corrected for the interannual trend of 2.06 ppm/year (Guerlet et al., 2013).

In June of year preceding the wildfire event, the XCO_2 values in 2009 and 2010 were nearly the same along latitude bands from 10° to 70°N in the Northern Hemisphere and exceeded the interannual trend by 0.5–1.5 ppm (Fig. 6a). These increased values relative to the trend may be caused by different rates of CO_2 absorption by vegetation, due to delayed or accelerated spring seasonal changes. The model runs using the four fluxes and the GOSAT retrieval are consistent.

Table 2
Correlation coefficients and biases derived from XCO_2 modeled using Prior + GV and LMDZ fluxes against retrievals by GOSAT L2, for the different latitudinal bands.

Latitudinal band (°N)	Number of points	Correlation coefficient		Average bias, ppm	
		Prior + GV	LMDZ	Prior + GV	LMDZ
55–60	2680	0.96	0.97	1.04	1.08
60–65	2903	0.95	0.97	0.92	1.42
65–70	2648	0.97	0.97	1.85	1.99
70–75	668	0.91	0.95	2.99	3.28
All bands	8899	0.95	0.96	1.70	1.94

The wildfire event in Central Russia started in July. The GOSAT L2 data show enhanced XCO_2 at latitudes 40°–80°N (Fig. 6b). The NIES TM with Prior + GV + GOSAT, LMDZ and the GELCA-EOF fluxes capture this effect for the central part of the burned area in the 55°–60°N band. These model runs show CO_2 transported northward with enhanced concentration near Novaya Zemlya (Fig. 7). This is in agreement with wind direction calculated using the National Centers for Environmental Prediction Global Forecast System (NCEP GFS) (Grumm, 2011). In general, the differences between XCO_2 distributions in July 2010 and July 2009 show three peaks of XCO_2 over North America, northern Europe, and the Far East (Fig. 7). The Far East region is prominent due to its high emission intensity, which is well captured by the model runs.

The peak of the event occurred in August, when XCO_2 was enhanced by 2.5 ppm relative to 2009 values over the forest fire regions (50°–65°N), and by

Table 3
Seasonal amplitude of XCO_2 for the different latitudinal bands, modeled using Prior + GV, Prior + GV + GOSAT, LMDZ, and GELCA-EOF fluxes, and derived from GOSAT Level 2 data, for 2009–2010.

Latitudinal band (°N)	Seasonal amplitude for 2009, ppm					Seasonal amplitude for 2010, ppm				
	GOSAT	Prior + GV	Prior + GV + GOSAT	LMDZ	GELCA-EOF	GOSAT	Prior + GV	Prior + GV + GOSAT	LMDZ	GELCA-EOF
55–60	8.92	8.79	8.32	7.29	8.62	14.35	9.65	8.83	8.49	7.91
60–65	10.31	8.44	8.48	8.21	8.79	11.34	11.05	10.49	9.05	8.96
65–70	10.42	8.93	8.88	8.74	8.71	11.91	9.83	9.28	9.31	8.84
70–75	10.21	6.35	6.84	7.34	6.38	5.61	4.62	4.59	5.25	3.61

2 ppm over the 40°–50°N and 65°–70°N bands, into which combustion products were transported (Fig. 6c). The model with all considered fluxes described the peak well, except that GELCA-EOF values are 0.5–1.0 ppm higher than other modeled and closer to observed XCO_2. At the end of August, the wind changed direction (Grumm, 2011), and the enhanced XCO_2 was transported mainly eastward. At the same time, enhanced fire activity in the USA and Canada led to elevated XCO_2 over the North Atlantic (Fig. 8).

In accordance with the differences between XCO_2 distributions in August 2010 and August 2009, we can identify only two regions of enhanced XCO_2 (North America, northern Europe), as the forest fires in the Far East had mainly ended.

In September, the forest fire event had almost ended due to autumn rains. However, the released CO_2 had accumulated in the free troposphere, and was detected by GOSAT (Fig. 6d). Dispersion of substances in the free troposphere is a slow process, and even in October, enhanced CO_2 concentrations were observed (Fig. 6e).

3.5. Comparison of GELCA-EOF fluxes for June–August, 2009 and 2010

In previous section GELCA-EOF system shown ability to invert CO_2 fluxes, which successfully described significant interannual variation of CO_2 uptake during the Northern Hemisphere summer between 2009 and 2010. Thus, our further study concentrated on analysis of GELCA-EOF fluxes. Table 4 shows the differences in CO_2 fluxes obtained using the GELCA-EOF inversion system between the periods June–August 2010 and June–August 2009. The difference is calculated for Western and Eastern hemispheres over land only, averaged over 5° bands.

Analyses of the GELCA-EOF data show marked differences in summer fluxes between 2010 and 2009 for the Western and Eastern hemispheres (Table 4). In the 50–55° and 55–60°N bands, which contain the forest fire regions, the additional CO_2 emission in 2010, as compared with that in 2009, is 22.58%–40.40%, while for bands located farther north, the growth is weaker or even negative. This confirms that the high concentrations of CO_2 at high latitudes in the summer of 2010 were caused by wildfires in central western Russia, the USA, and Canada.

Table 5 shows estimates of flux differences for the same period, but using only ground-based observations without GOSAT as in Prior + GV. Use of GOSAT data has a substantial impact on the estimation of the level of additional CO_2 emission due to forest fires in the 50°–60°N band in the Eastern Hemisphere, as fluxes estimated with the GOSAT data are 0.4–0.6 GtC/yr higher than those estimated without such data (see difference of values in Tables 4 and 5).

The CO_2 fluxes in the northern part of the Western Hemisphere are successfully constrained by observations from ground-based sites located in the temperate zone. The disparity between 2009 and 2010 fluxes estimated with and without GOSAT data is no more than ~7%. Thus, here the GOSAT data have a substantial impact only in the 65–75°N band, where the constraints of ground-based observations are weaker.

4. Discussion

The increase of CO_2 mixing ratio in summer of 2010 may be effect not only of fires, but also of enhancement of biospheric respiration induced by the high temperature. However, the value of carbon released due to wild fires in Russia in 2010 was extremely high. This year emission (2.12 kgC/m^2/yr) exceeds averaged value for 1998–2010 (1.47 kgC/m^2/yr) calculated for all land cover types (Shvidenko et al., 2011). While the total burned area in 2010 was slightly below the long term average.

The XCO_2 modeled with Prior + GV and LMDZ fluxes captures only a part of the IAV of CO_2 caused by the fire event during summer 2010 (Fig. 6). Apparently, the footprints of the selected observations sites in correspondent inversions did not cover enough of the

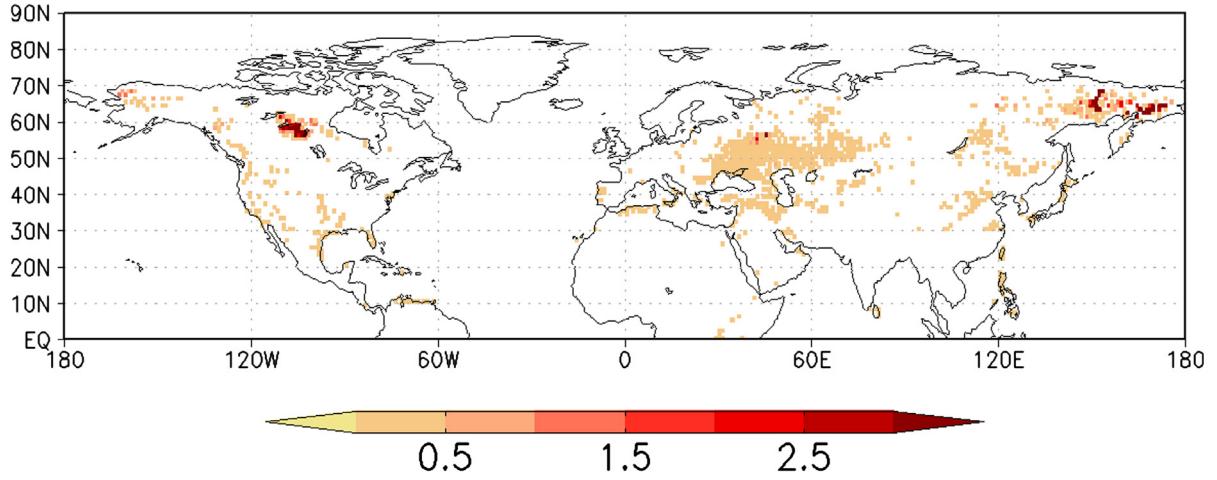

Fig. 5. Forest fire emissions (gC/m^2/day) in the Northern Hemisphere derived from the GFED database for July 2010 (van der Werf et al., 2010).

burned area. Indeed combustion products from wildfires were mainly transported to the regions poorly covered by ground-based observations (the Northern and Eastern parts of Russia, the Atlantic Ocean (Fig. 8)). It seems, the GFED forest fire product used as a component of *a priori* fluxes adequately characterizes the location of the burned area, but it may underestimate emissions (Guerlet et al., 2013).

In general, a joint inversion of GOSAT and surface data is more successful in estimation of XCO_2 IAV in the Northern Hemisphere. The comparisons show that the inversion with the advanced GELCA-EOF system has benefits compared with the standard regional Prior + GV + GOSAT method in northern high-latitude regions, because grid-based fluxes are estimated without discontinuities at regional boundaries,

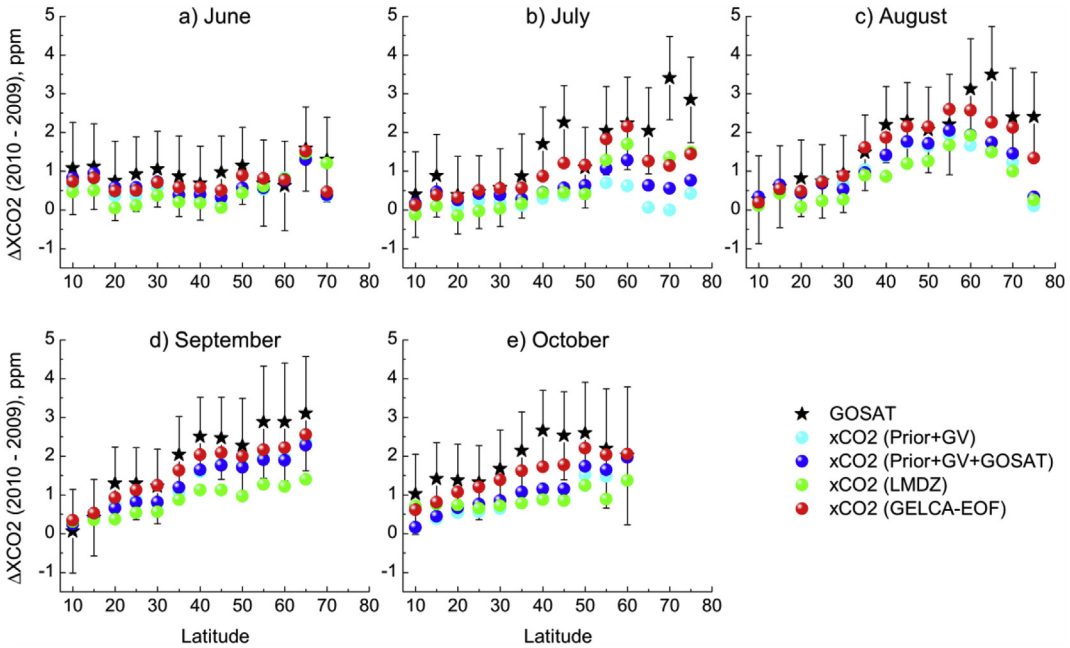

Fig. 6. XCO_2 values for June–October 2010 minus those for June–October 2009 (shown as 5°-band averages). The interannual trend of 2.06 ppm/year has been removed. The black stars are XCO_2 values, as derived from GOSAT data analysis with GOSAT L2 retrieval. The error bars represent the error of the mean. Colored circles represent XCO_2 calculated by NIES TM using Prior + GV (cyan), Prior + GV + GOSAT (blue), LMDZ (green), and GELCA-EOF (red). (For interpretation of the references to color in this figure legend, the reader is referred to the web version of this article.)

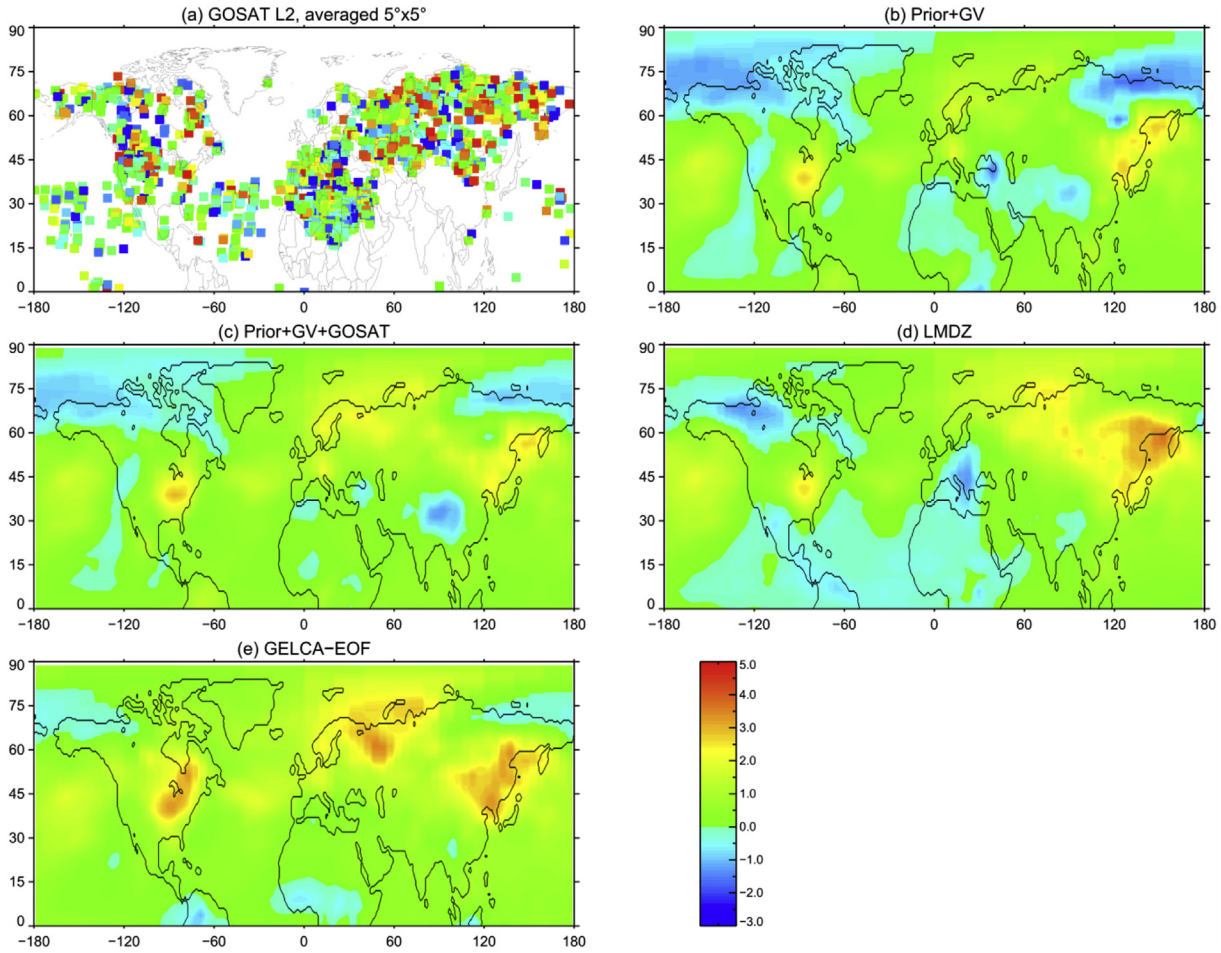

Fig. 7. Differences between XCO_2 in July 2010 and July 2009, for the region 0°–90°N, derived from: a) GOSAT L2 (shown as averaged over 5° × 5° grids) and NIES TM simulations, and the same with b) Prior + GV, c) Prior + GV + GOSAT, d) LMDZ, and e) GELCA-EOF fluxes. The interannual trend of 2.06 ppm/year has been removed.

and because this inversion uses the more sophisticated and higher-resolution transport model GELCA. Moreover, the GELCA-EOF system utilizes column-averaged observations by GOSAT without aggregation, which increases their accuracy. As results, difference in XCO_2 calculated with GELCA-EOF and Prior + GV + GOSAT fluxes is about 0.5 ppm in average (Fig. 6). More detailed comparison of Prior + GV + GOSAT and GELCA-EOF methods is required additional study, which is out of scope of the paper.

To cover gaps in Prior + GV and Prior + GV + GOSAT fluxes we used unoptimized *a priori* fluxes in simulations for periods 1 January – 31 May 2009 and 1 November to 31 December 2010. However, it should not distort our analysis, because optimized fluxes are available for boreal summer seasons 2009 and 2010, when *a priori* CO_2 emission has high level of inaccuracy due to uncertainty in biospheric uptake and required to be optimized.

5. Conclusion

The distribution of XCO_2 in the subarctic was investigated using the NIES TM and the GOSAT L2 products. We performed XCO_2 simulations for the period 2009–2010 using the NIES TM with four flux datasets. The Prior + GV and LMDZ flux sets are optimized only with surface observations, while the Prior + GV + GOSAT and GELCA-EOF flux sets are based on both surface and GOSAT L2 observations, but represent different approaches to the treatment of the retrieved data.

Comparisons of modeled XCO_2 with XCO_2 observations from ground-based high-resolution FTS observations collected at two of the northernmost sites,

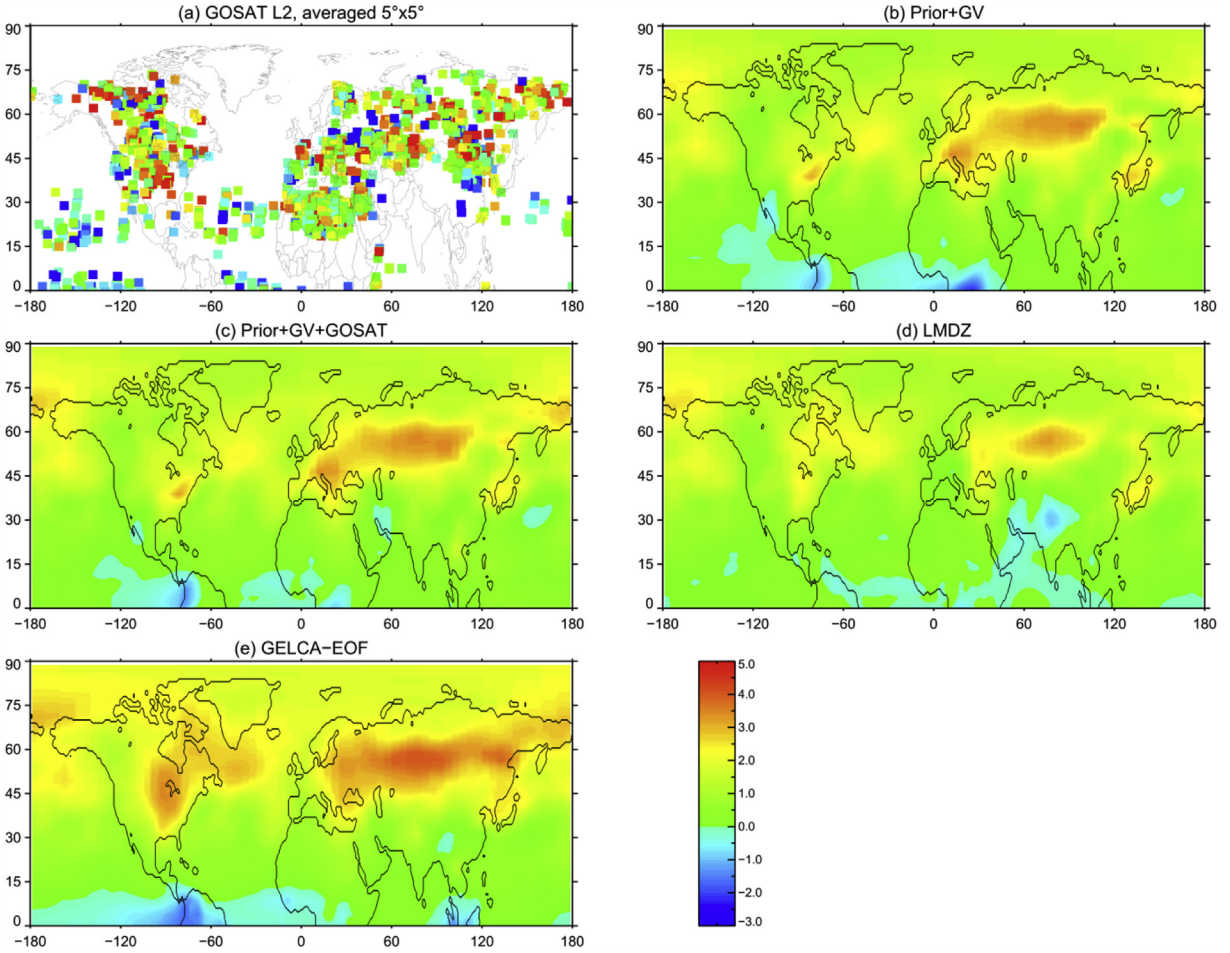

Fig. 8. Same as Fig. 7, but for August.

Ny Ålesund and Sodankylä, revealed a performance improvement as compared with the simulation using unoptimized fluxes (Belikov et al., 2013b).

Fluxes optimized without GOSAT retrievals (Prior + GV and LMDZ) were compared directly with GOSAT L2 data. Selected coincident points were averaged over four latitudinal 5° bands in high-latitude regions of the Northern Hemisphere. Correlation coefficients of 0.95–0.96, and average bias values of 1.70–1.94 ppm, were obtained, demonstrating the consistency of the datasets. Although the results are fairly coarse, the agreement of the model results is quite reasonable over such a large area that is not covered by any other measurements. Moreover, the CO_2 seasonality is abnormally in summer of 2010.

Table 4
Difference in CO_2 fluxes (GtC/yr and % compared to 2009) obtained using the GELCA-EOF inversion system, for the period June–August 2010 minus June–August 2009 (shown as 5°-band averages). Differences are calculated for Western and Eastern Hemispheres over land only. Ground-based observations and GOSAT L2 data are used.

Latitudinal band (°N)	Difference in CO_2 fluxes			
	Western Hemisphere		Eastern Hemisphere	
	GtC/yr	%	GtC/yr	%
50–55	0.5363	26.61	1.0759	39.85
55–60	0.4235	40.40	0.8927	22.58
60–65	−0.0084	−2.16	0.4163	11.61
65–70	−0.0233	−19.30	0.1200	12.66
70–75	−0.0021	−5.18	0.0078	7.64

The impact on CO_2 levels of emissions from enhancement of biospheric respiration induced by the high temperature and strong wildfires occurring in the summer of 2010 was analyzed using the NIES TM simulations with considered fluxes. The massive CO_2 transport into subarctic and Arctic regions mainly caused by wildfires in central western Russia, the USA, and Canada was found. Using NIES TM with GELCA-EOF fluxes during the peak of the wildfire event in

Table 5
Same as Table 4, but only ground-based observations are used.

Latitudinal band (°N)	Difference in CO_2 fluxes			
	Western Hemisphere		Eastern Hemisphere	
	GtC/yr	%	GtC/yr	%
50–55	0.3564	20.34	0.3818	14.44
55–60	0.3885	43.55	0.4937	14.12
60–65	0.0149	4.93	0.4670	15.85
65–70	−0.0081	−7.96	0.1339	17.47
70–75	0.0040	9.94	0.0071	7.62

August 2010, we detected XCO_2 enhancement of 2.5 ppm relative to 2009 over forest fire regions (50°–65°N), and of 2 ppm over 65°–70°N band, into which combustion products were transported. Use of GOSAT data has a substantial impact on estimates of the level of additional CO_2 emission due to forest fires between 50°N and 60°N in the Eastern Hemisphere, as fluxes estimated with the GOSAT data are higher by ~0.4–0.6 GtC/yr. However, CO_2 fluxes in the northern part of the Western Hemisphere are successfully constrained by observations from ground-based sites located in the temperate zone. Here, the difference in fluxes estimated with and without GOSAT data is less than 0.2 GtC/yr.

The XCO_2 modeled with fluxes obtained without GOSAT data (Prior + GV and LMDZ) captures only a part of the IAV of CO_2 during summer 2010. As the GFED forest fire product used as a component of *a priori* fluxes adequately characterizes the location of burned areas, but it underestimates the emissions. Thus, we have shown the implementation of GOSAT data for studying the carbon cycle in the subarctic. The results reveal the benefits of XCO_2 GOSAT data use to evaluate modeled results, and to provide an additional constraint during inverse model flux optimization. The GOSAT NIES Level 2 data products are under constant development. A longer retrieval period, an enhanced number of scenes, and reduced standard deviations and biases of the data due to the implementation of more sophisticated retrieval algorithms, as well as improvements in the inversion scheme, will allow us to address in more detail the problems identified in this study in future work.

Acknowledgments

The authors would like to thank the GRENE-Arctic Project and the members of the GOSAT Project for their contribution to this work. The GOSAT Project is a joint undertaking of three organizations: the Japan Aerospace Exploration Agency (JAXA), the National Institute for Environmental Studies (NIES), and the Japanese Ministry of the Environment (MOE). We thank Frederic Chevallier for providing LMDZ CO_2 flux data. The JRA-25/JCDAS datasets used in this study were provided by the Japan Meteorological Agency. We also thank the authors of GLOBALVIEW-CO_2 and TCCON for the observational data. The NIES TM numerical simulations were performed on the NIES supercomputer system (NEC SX-8R/128M16).

References

Andres, R.J., Boden, T.A., Marland, G., 2009. Annual Fossil-fuel CO_2 Emissions: Mass of Emissions Gridded by One Degree Latitude by One Degree Longitude. Carbon Dioxide Information Analysis Center, Oak Ridge National Laboratory, U.S. Department of Energy, Oak Ridge, Tenn., U.S.A. http://dx.doi.org/10.3334/CDIAC/ffe.ndp058.2009.

Andres, R.J., Gregg, J.S., Losey, L., Marland, G., Boden, T., 2011. Monthly, global emissions of carbon dioxide from fossil fuel consumption. Tellus 63B, 309–327.

Barnaba, F., Angelini, F., Curci, G., Gobbi, G.P., 2011. An important fingerprint of wildfires on the European aerosol load. Atmos. Chem. Phys. 11, 10487–10501.

Basu, S., Guerlet, S., Butz, A., Houweling, S., Hasekamp, O., Aben, I., Krummel, P., Steele, P., Langenfelds, R., Torn, M., Biraud, S., Stephens, B., Andrews, A., Worthy, D., 2013. Global CO_2 fluxes estimated from GOSAT retrievals of total column CO_2. Atmos. Chem. Phys. Discuss. 13, 4535–4600. http://dx.doi.org/10.5194/acpd-13-4535-2013.

Belikov, D., Maksyutov, S., Miyasaka, T., Saeki, T., Zhuravlev, R., Kiryushov, B., 2011. Mass-conserving tracer transport modelling on a reduced latitude–longitude grid with NIES-TM. Geosci. Model Dev. 4, 207–222.

Belikov, D.A., Maksyutov, S., Krol, M., Fraser, A., Rigby, M., Bian, H., Agusti-Panareda, A., Bergmann, D., Bousquet, P., Cameron-Smith, P., Chipperfield, M.P., Fortems-Cheiney, A., Gloor, E., Haynes, K., Hess, P., Houweling, S., Kawa, S.R., Law, R.M., Loh, Z., Meng, L., Palmer, P.I., Patra, P.K., Prinn, R.G., Saito, R., Wilson, C., 2013a. Off-line algorithm for calculation of vertical tracer transport in the troposphere due to deep convection. Atmos. Chem. Phys. 13, 1093–1114. http://dx.doi.org/10.5194/acp-13-1093-2013.

Belikov, D., Maksyutov, S., Sherlock, V., Aoki, S., Deutscher, N.M., Dohe, S., Griffith, D., Kyro, E., Morino, I., Nakazawa, T., Notholt, J., Rettinger, M., Schneider, M., Sussmann, R., Toon, G.C., Wennberg, P.O., Wunch, D., 2013b. Simulations of column-average CO_2 and CH_4 using the NIES TM with a hybrid sigma–isentropic ($\sigma-\theta$) vertical coordinate. Atmos. Chem. Phys. 13, 1713–1732. http://dx.doi.org/10.5194/acp-13-1713-2013.

Bousquet, P., Peylin, P., Ciais, P., Le Quéré, C., Friedlingstein, P., Tans, P.P., 2000. Regional changes in carbon dioxide fluxes of land and oceans since 1980. Science 290, 1342–1346.

Brown, J., Ferrians, O.J., Heginbottom, J.A., Melnikov, E.S., 1997. Circum-arctic Map of Permafrost and Ground-ice Conditions. U.S. Geol. Surv, Washington DC. Circum-Pacific Map, CP-45.

Chevallier, F., Ciais, P., Conway, T.J., Aalto, T., Anderson, B.E., Bousquet, P., Brunke, E.G., Ciattaglia, L., Esaki, Y., Frohlich, M.,

Gomez, A., Gomez-Pelaez, A.J., Haszpra, L., Krummel, P.B., Langenfelds, R.L., Leuenberger, M., Machida, T., Maignan, F., Matsueda, H., Morguí, J.A., Mukai, H., Nakazawa, T., Peylin, P., Ramonet, M., Rivier, L., Sawa, Y., Schmidt, M., Steele, L.P., Vay, S.A., Vermeulen, A.T., Wofsy, S., Worthy, D., 2010. CO_2 surface fluxes at grid point scale estimated from a global 21 year reanalysis of atmospheric measurements. J. Geophys. Res. 115, D21307. http://dx.doi.org/10.1029/2010JD013887.

Cogan, A.J., Boesch, H., Parker, R.J., Feng, L., Palmer, P.I., Blavier, J.-F.L., Deutscher, N.M., Macatangay, R., Notholt, J., Roehl, C., Warneke, T., Wunch, D., 2012. Atmospheric carbon-dioxide retrieved from the Greenhouse gases Observing SATellite (GOSAT): comparison with ground-based TCCON observations and GEOS-Chem model calculations. J. Geophys. Res. 117, D21301. http://dx.doi.org/10.1029/2012JD018087.

Ganshin, A., Oda, T., Saito, M., Maksyutov, S., Valsala, V., Andres, R.J., Fisher, R.E., Lowry, D., Lukyanov, A., Matsueda, H., Nisbet, E.G., Rigby, M., Sawa, Y., Toumi, R., Tsuboi, K., Varlagin, A., Zhuravlev, R., 2012. A global coupled Eulerian-Lagrangian model and 1 × 1 km CO_2 surface flux dataset for high-resolution atmospheric CO_2 transport simulations. Geosci. Model Dev. 5, 231–243.

GLOBALVIEW-CO, 2011. Cooperative Atmospheric Data Integration Project – Carbon Dioxide. CD-ROM, NOAA ESRL, Boulder, Colorado (Also available on Internet via anonymous FTP to. ftp.cmdl.noaa.gov. Path: ccg/co2/GLOBALVIEW).

Gloor, M., Fan, S.-M., Pacala, S., Sarmiento, J., 2000. Optimal sampling of the atmosphere for purpose of inverse modeling: a model study. Global biogeochem. Cycles 14 (1), 407–428. http://dx.doi.org/10.1029/1999GB900052.

Graven, H.D., Keeling, R.F., Piper, S.C., Patra, P.K., Stephens, B.B., Wofsy, S.C., Welp, L.R., Sweeney, C., Tans, P.P., Kelley, J.J., Daube, B.C., Kort, E.A., Santoni, G.W., Bent, J.D., 2013. Enhanced seasonal exchange of CO_2 by northern ecosystems since 1960. Science 341, 1239207. http://dx.doi.org/10.1126/science.1239207.

Grumm, R.H., 2011. The Central european and russian heat event of July–August 2010. Bull. Amer. Meteorol. Soc. 92, 1285–1296. http://dx.doi.org/10.1175/2011BAMS3174.1.

Guerlet, S., Basu, S., Butz, A., Krol, M., Hahne, P., Houweling, S., Hasekamp, O.P., Aben, I., 2013. Reduced carbon uptake during the 2010 Northern Hemisphere summer from GOSAT. Geophys. Res. Lett. 40, 2378–2383. http://dx.doi.org/10.1002/grl.50402.

Gurney, K.R., Law, R.M., Denning, A.S., Rayner, P.J., Baker, D., Bousquet, P., Bruhwiler, L., Chen, Y.-H., Ciais, P., Fan, S., Fung, I.Y., Gloor, M., Heimann, M., Higuchi, K., John, J., Maki, T., Maksyutov, S., Masarie, K., Peylin, P., Prather, M., Pak, B.C., Randerson, J., Sarmiento, J., Taguchi, S., Takahashi, T., Yuen, C.-W., 2002. Towards robust regional estimates of CO_2 sources and sinks using atmospheric transport models. Nature 415, 626–630.

Hack, J.J., Boville, B.A., Briegleb, B.P., Kiehl, J.T., Rasch, P.J., Williamson, D.L., 1993. Description of the NCAR Community Climate Model (CCM2). NCAR Tech. Note, NCAR/TN-382. NCAR, Boulder, CO.

Heimann, M., Keeling, C., 1989. A three-dimensional model of atmospheric CO_2 transport based on observed winds: 2: model description and simulated tracer experiments. In: Peterson, D.H. (Ed.), Aspects of Climate Variability in the Pacific and the Western Americas, Geophysical Monograph 55. AGU, Washington, pp. 237–275.

Ito, A., 2010. Changing ecophysiological processes and carbon budget in East Asian ecosystems under near-future changes in climate: Implications for long-term monitoring from a process-based model. J. Plant Res. 123, 577–588.

Konovalov, I.B., Beekmann, M., Kuznetsova, I.N., Yurova, A., Zvyagintsev, A.M., 2011. Atmospheric impacts of the 2010 Russian wildfires: integrating modelling and measurements of an extreme air pollution episode in the Moscow region. Atmos. Chem. Phys. 11, 10031–10056. http://dx.doi.org/10.5194/acp-11-10031-2011.

Koven, C.D., Ringeval, B., Friedlingstein, P., Ciais, P., Cadule, P., Khvorostyanov, D., Krinner, G., Tarnocai, C., 2011. Permafrost carbon-climate feedbacks accelerate global warming. P. Natl. Acad. Sci. USA 108, 14769–14774.

Kuze, A., Suto, H., Nakajima, M., Hamazaki, T., 2009. Thermal and near infrared sensor for carbon observation Fourier-transform spectrometer on the Greenhouse Gases Observing Satellite for greenhouse gases monitoring. Appl. Opt. 48, 6716–6733. http://dx.doi.org/10.1364/AO.48.006716.

Maksyutov, S., Takagi, H., Belikov, D.A., Saeki, T., Zhuravlev, R., Ganshin, A., Lukyanov, A., Yoshida, Y., Oshchepkov, S., Bril, A., Saito, M., Oda, T., Valsala, V.K., Saito, R., Andres, R.J., Conway, T., Tans, P., Yokota, T., 2012. Estimation of regional surface CO_2, fluxes with GOSAT observations using two inverse modeling approaches. In: Proc. SPIE 8529, Remote Sensing and Modeling of the Atmosphere, Oceans, and Interactions IV, p. 85290G. http://dx.doi.org/10.1117/12.979664.

Maksyutov, S., Takagi, H., Valsala, V.K., Saito, M., Oda, T., Saeki, T., Belikov, D.A., Saito, R., Ito, A., Yoshida, Y., Morino, I., Uchino, O., Andres, R.J., Yokota, T., 2013. Regional CO_2 flux estimates for 2009–2010 based on GOSAT and ground-based CO_2 observations. Atmos. Chem. Phys. 13, 9351–9373. http://dx.doi.org/10.5194/acp-13-9351-2013.

Muskett, R., 2013. GOSAT CH_4 and CO_2, MODIS evapotranspiration on the Northern Hemisphere June and July 2009, 2010 and 2011. Atmos. Clim. Sci. 3, 177–185. http://dx.doi.org/10.4236/acs.2013.32019.

Oda, T., Maksyutov, S., 2011. A very high-resolution (1 km × 1 km) global fossil fuel CO_2 emission inventory derived using a point source database and satellite observations of nighttime lights. Atmos. Chem. Phys. 11, 543–556.

Onogi, K., Tsutsui, J., Koide, H., Sakamoto, M., Kobayashi, S., Hatsushika, H., Matsumoto, T., Yamazaki, N., Kamahori, H., Takahashi, K., Kadokura, S., Wada, K., Kato, K., Oyama, R., Ose, T., Mannoji, N., Taira, R., 2007. The JRA-25 reanalysis. J. Meteorol. Soc. Jpn. 85, 369–432.

Oshchepkov, S., Bril, A., Yokota, T., Morino, I., Yoshida, Y., Matsunaga, T., Belikov, D., Wunch, D., Wennberg, P., Toon, G., O'Dell, C., Butz, A., Guerlet, S., Cogan, A., Boesch, H., Eguchi, N., Deutscher, N., Griffith, D., Macatangay, R., Notholt, J., Sussmann, R., Rettinger, M., Sherlock, V., Robinson, J., Kyrö, E., Heikkinen, P., Feist, D.G., Nagahama, T., Kadygrov, N., Maksyutov, S., Uchino, O., Watanabe, H., 2012. Effects of atmospheric light scattering on spectroscopic observations of greenhouse gases from space: validation of PPDF-based CO_2 retrievals from GOSAT. J. Geophys. Res. 117, D12305. http://dx.doi.org/10.1029/2012JD017505.

Oshchepkov, S., Bril, A., Yokota, T., Wennberg, P.O., Deutscher, N.M., Wunch, D., Toon, G.C., Yoshida, Y., O'Dell, C.W., Crisp, D., Miller, C.E., Frankenberg, C., Butz, A., Aben, I., Guerlet, S., Hasekamp, O., Boesch, H., Cogan, A., Parker, R., Griffith, D., Macatangay, R., Notholt, J.,

Sussmann, R., Rettinger, M., Sherlock, V., Robinson, J., Kyro, E., Heikkinen, P., Feist, D.G., Morino, I., Kadygrov, N., Belikov, D., Maksyutov, S., Matsunaga, T., Uchino, O., Watanabe, H., 2013. Effects of atmospheric light scattering on spectroscopic observations of greenhouse gases from space. Part 2: algorithm intercomparison in the GOSAT data processing for CO_2 retrievals over TCCON sites. J. Geophys. Res. Atmos. 118, 1493−1512. http://dx.doi.org/10.1002/jgrd.50146.

Patra, P.K., Ishizawa, M., Maksyutov, S., Nakazawa, T., Inoue, G., 2005. Role of biomass burning and climate anomalies for land-atmosphere carbon fluxes based on inverse modeling of atmospheric CO_2. Glob. Biogeochem. Cycles 19, GB3005. http://dx.doi.org/10.1029/2004GB002258.

Peters, W., Jacobson, A.R., Sweeney, C., Andrews, A.E., Conway, T.J., Masarie, K., Miller, J.B., Bruhwiler, L.M.P., Pétron, G., Hirsch, A.I., Worthy, D.E.J., van der Werf, G.R., Randerson, J.T., Wennberg, P.O., Krol, M.C., Tans, P.P., 2007. An atmospheric perspective on North American carbon dioxide exchange: carbon tracker. P. Natl. Acad. Sci. USA 104, 18925−18930.

Portin, H., Mielonen, T., Leskinen, A., Arola, A., Pärjälä, E., Romakkaniemi, S., Laaksonen, A., Lehtinen, K.E.J., Komppula, M., 2012. Biomass burning aerosols observed in Eastern Finland during the Russian wildfires in summer 2010 − part 1: in-situ aerosol characterization. Atmos. Environ. 47, 269−278.

Rayner, P.J., O'Brien, D.M., 2001. The utility of remotely sensed CO_2 concentration data in surface source inversions. Geophys. Res. Lett. 28, 175−178.

Reid, J.S., Koppmann, R., Eck, T.F., Eleuterio, D.P., 2005. A review of biomass burning emissions part II: intensive physical properties of biomass burning particles. Atmos. Chem. Phys. 5, 799−825.

Saeki, T., Maksyutov, S., Saito, M., Valsala, V., Oda, T., Andres, R.J., Belikov, D.A., Tans, P., Dlugokencky, E., Yoshida, Y., Morino, I., Uchino, O., Yokota, T., 2013. Inverse modeling of CO_2 fluxes using GOSAT data and multi-year ground-based observations. SOLA 9, 45−50. http://dx.doi.org/10.2151/sola.2013-011.

Saito, M., Ito, A., Maksyutov, S., 2011. Evaluation of biases in JRA-25/JCDAS precipitation and their impact on the global terrestrial carbon balance. J. Clim. 24, 4109−4125.

Saito, M., Ito, A., Maksyutov, S., 2013. Synthesis modeling of atmospheric CO_2 variability and terrestrial biomass with inversion scheme. Geosci. Model Dev. Discuss. 6, 4243−4280.

Schuur, E.A.G., Vogel, J.G., Crummer, K.G., Lee, H., Sickman, J.O., Osterkamp, T.E., 2009. The effect of permafrost thaw on old carbon release and net carbon exchange from tundra. Nature 459, 556−559.

Shvidenko, A.Z., Schepaschenko, D.G., Vaganov, E.A., Sukhinin, A.I., Maksyutov, S.S., McCallum, I., Lakyda, I.P., 2011. Impact of wildfire in Russia between 1998−2010 on ecosystems and the global carbon budget. Doklady Earth Sci. 441 (2), 1678−1682.

Sitnov, S.A., 2011. Aerosol optical thickness and the total carbon monoxide content over the European Russia territory in the 2010 summer period of mass fires: interrelation between the variation in pollutants and meteorological parameters. Izvestiya, Atmos. Oceanic Phys. 47, 714−728.

Stohl, A., Forster, C., Frank, A., Seibert, P., Wotawa, G., 2005. Technical note: the Lagrangian particle dispersion model FLEXPART version 6.2. Atmos. Chem. Phys. 5, 2461−2474.

Stohl, A., Andrews, E., Burkhart, J.F., Forster, C., Herber, A., Hoch, S.W., Kowal, D., Lunder, C., Mefford, T., Ogren, J.A., Sharma, S., Spichtinger, N., Stebel, K., Stone, R., Ström, J., Tørseth, K., Wehrli, C., Yttri, K.E., 2006. Pan-Arctic enhancements of light absorbing aerosol concentrations due to North American boreal forest fires during summer 2004. J. Geophys. Res. 111, D22214. http://dx.doi.org/10.1029/2006JD007216.

Stohl, A., Berg, T., Burkhart, J.F., Fjæraa, A.M., Forster, C., Herber, A., Hov, Ø., Lunder, C., McMillan, W.W., Oltmans, S., Shiobara, M., Simpson, D., Solberg, S., Stebel, K., Ström, J., Tørseth, K., Treffeisen, R., Virkkunen, K., Yttri, K.E., 2007. Arctic smoke − record high air pollution levels in the European Arctic due to agricultural fires in Eastern Europe in spring 2006. Atmos. Chem. Phys. 7, 511−534.

Takagi, H., Saeki, T., Oda, T., Saito, M., Valsala, V., Belikov, D., Saito, R., Yoshida, Y., Morino, I., Uchino, O., Andres, R.J., Yokota, T., Maksyutov, S., 2011. On the benefit of GOSAT observations to the estimation of regional CO_2 fluxes. SOLA 7, 161−164.

Valsala, V., Maksyutov, S., 2010. Simulation and assimilation of global ocean pCO_2 and air−sea CO2 fluxes using ship observations of surface ocean pCO_2 in a simplified biogeochemical offline model. Tellus 62B, 821−840. http://dx.doi.org/10.1111/j.1600-0889.2010.00495.x.

van der Werf, G.R., Randerson, J.T., Giglio, L., Collatz, G.J., Mu, M., Kasibhatla, P.S., Morton, D.C., DeFries, R.S., Jin, Y., van Leeuwen, T.T., 2010. Global fire emissions and the contribution of deforestation, savanna, forest, agricultural, and peat fires (1997−2009). Atmos. Chem. Phys. 10, 11707−11735.

van Leer, B., 1977. Towards the ultimate conservative difference scheme. IV: a new approach to numerical convection. J. Comput. Physiol. 23, 276−299.

Witte, J.C., Douglass, A.R., da Silva, A., Torres, O., Levy, R., Duncan, B.N., 2011. NASA A-Train and Terra observations of the 2010 Russian wildfires. Atmos. Chem. Phys. 11, 9287−9301. http://dx.doi.org/10.5194/acp-11-9287-2011.

Wunch, D., Toon, G.C., Blavier, J.-F.L., Washenfelder, R.A., Notholt, J., Connor, B.J., Griffith, D.W.T., Sherlock, V., Wennberg, P.O., 2011. The total carbon column observing network. Phil. Trans. R. Soc. A 369, 2087−2112. http://dx.doi.org/10.1098/rsta.2010.0240.

Yokota, T., Yoshida, Y., Eguchi, N., Ota, Y., Tanaka, T., Watanabe, H., Maksyutov, S., 2009. Global concentrations of CO_2 and CH_4 retrieved from GOSAT: first preliminary results. SOLA 5, 160−163. http://dx.doi.org/10.2151/sola.2009-041.

Yoshida, Y., Ota, Y., Eguchi, N., Kikuchi, N., Nobuta, K., Tran, H., Morino, I., Yokota, T., 2011. Retrieval algorithm for CO_2 and CH_4 column abundances from short-wavelength infrared spectral observations by the Greenhouse gases observing satellite. Atmos. Meas. Tech. 4, 717−734.

Yoshida, Y., Kikuchi, N., Yokota, T., 2012. On-orbit radiometric calibration of SWIR bands of TANSO-FTS onboard GOSAT. Atmos. Meas. Tech. 5, 2515−2523. http://dx.doi.org/10.5194/amt-5-2515-2012.

Yoshida, Y., Kikuchi, N., Morino, I., Uchino, O., Oshchepkov, S., Bril, A., Saeki, T., Schutgens, N., Toon, G.C., Wunch, D., Roehl, C.M., Wennberg, P.O., Griffith, D.W.T., Deutscher, N.M., Warneke, T., Notholt, J., Robinson, J., Sherlock, V., Connor, B., Rettinger, M., Sussmann, R., Ahonen, P., Heikkinen, P., Kyrö, E., Mendonca, J., Strong, K., Hase, F., Dohe, S., Yokota, T., 2013. Improvement of the retrieval algorithm for GOSAT SWIR XCO_2 and XCH_4 and

their validation using TCCON data. Atmos. Meas. Tech. 6, 1533–1547. http://dx.doi.org/10.5194/amt-6-1533-2013.

Zhuravlev, R., Khattatov, B., Kiryushov, B., Maksyutov, S., 2011. Technical Note: a novel approach to estimation of time-variable surface sources and sinks of carbon dioxide using empirical orthogonal functions and the Kalman filter. Atmos. Chem. Phys. 11, 10305–10315. http://dx.doi.org/10.5194/acp-11-10305-2011.

Zhuravlev, R.V., Ganshin, A.V., Maksyutov, S.S., Oshchepkov, S.L., Khattatov, B.V., 2013. Estimation of global fluxes of CO_2 using ground-station and satellite (GOSAT) observation data with empirical orthogonal functions. Atmos. Oceanic Opt. 2013 (26), 388–397.